ARTICLE OPEN

Check for updates

# Enhancing low-dose radiotherapy efficacy with PARP inhibitors via FBL-mediated oxidative stress response in colorectal cancer

Ming Wen[1,2,3,4,5,13], Yanfang Qiu[1,2,6,13], Meng Wang[1,2], Feiyu Tang[1,2], Wenfeng Hu[1,2], Yongwei Zhu[7], Wenchao Zhao[1,2], Wenzhen Hu[1,2], Zhuohang Chen[1,2], Yumei Duan[8], Anke Geng[9], Fengbo Tan[10], Yuqiang Li[10], Qian Pei[10], Haiping Pei[10], Zhiyong Mao[9], Ningbo Wu[11], Lunquan Sun[1,2,3,4,5]✉ and Rong Tan[1,2,3,4,5,12]✉



The effectiveness of radiotherapy in colorectal cancer (CRC) relies on its ability to induce cell death via the generation of reactive oxygen species (ROS). However, genes responsible for mitigating oxidative stress can impede radiotherapy's efficacy. In this study, we elucidate a significant association between the nucleolar protein Fibrillarin (FBL) and the oxidative stress response in CRC tumors. Our findings reveal elevated expression of FBL in colorectal cancer, which positively correlates with oxidative stress levels. Mechanistically, FBL demonstrates direct accumulation at DNA damage sites under the regulation of PARP1. Specifically, the N-terminal GAR domain of FBL is susceptible to PARylation by PARP1, enabling FBL to recognize PARylated proteins. The accumulation of damaged FBL plays a pivotal role in facilitating short-patched base excision repair by recruiting Ligase III and disassociating PCNA and FEN1. Moreover, tumors with heightened FBL expression exhibit reduced DNA damage levels but increased sensitivity to combined low-dose radiotherapy and olaparib treatment. This underscores the potential of leveraging PARP inhibitors to augment radiotherapy sensitivity in CRC cases characterized by elevated FBL expression, offering a promising therapeutic avenue.

*Oncogene* (2025) 44:228–240; https://doi.org/10.1038/s41388-024-03207-w

## INTRODUCTION

Chemoradiotherapy is widely employed as a preoperative intervention for advanced rectal cancer, yet a significant proportion of patients, approximately 75%–80%, do not attain complete responses [1, 2]. This highlights the urgent need for precision-based strategies to enhance therapeutic outcomes in specific patient subsets. Radiotherapy eradicates cancer cells by producing reactive oxygen species (ROS) and inflicting DNA damage beyond the cell's repair capability. Consequently, identification of targets that mitigate oxidative stress could offer crucial insights into the mechanisms underlying radioresistance.

The intestine is characterized by its resident gut microbiota, active metabolism, and persistent inflammatory stresses. Oxidative stress, which stems from inflammation, high metabolic activity, and various internal and external factors, is recognized as a key threat to genomic integrity [3, 4]. Elevated levels of reactive oxygen species (ROS) preferentially target guanine-rich sequences in the genome, resulting in oxidized base lesions such as 8-oxo-7,8-dihydro-2′-deoxyguanosine (8-oxodG) or 8-hydroxy-2′-deoxyguanosine (8-OHdG). These lesions are detected and excised by oxidative DNA damage response (DDR) mechanisms and subsequently repaired through the base excision repair (BER) pathway. However, when oxidative damage surpasses the BER pathway's repair capacity, it can lead to the formation of single-strand or double-strand DNA breaks. The role of oxidative damage and the homeostasis of DNA damage repair in radiotherapeutic efficacy in colorectal cancer (CRC) is still not fully understood.

PARP1 is an enzyme with crucial roles in DNA damage repair and gene regulation. Upon DNA damage, PARP1 can be activated by damaged DNA, subsequently amplifying signal pathways by recruiting various substrates through poly(ADP-ribosyl)ation (PARylation). PARP inhibitors (PARPis) were initially identified as effective targets in ovarian and breast cancers with homologous recombination deficiency (HRD), leading to synthetic lethality [5]. However, the application of PARPi in other cancers, such as colorectal cancer, has been limited due to the low mutation frequency in the homologous recombination (HR) pathway. Mass spectrometry analyses have identified numerous additional proteins as PARP substrates in

[1]Department of Oncology, Xiangya Cancer Center, Xiangya Hospital, Central South University, Changsha 410008, China. [2]Key Laboratory of Molecular Radiation Oncology Hunan Province, Changsha 410008, China. [3]National Clinical Research Center for Geriatric Disorders, Xiangya Hospital, Changsha, Huan 410008, China. [4]Hunan International Science and Technology Collaboration Base of Precision Medicine for Cancer, Changsha 410008, China. [5]Center for Molecular Imaging of Central South University, Xiangya Hospital, Changsha 410008, China. [6]Hunan Cancer Hospital and The Affiliated Cancer Hospital of Xiangya School of Medicine, Central South University, Changsha, Hunan, China. [7]Hunan International Scientific and Technological Cooperation Base of Brain Tumor Research, Xiangya Hospital, Central South University, Changsha 410008, China. [8]Department of Pathology, Xiangya Hospital, Central South University, Changsha, Hunan, China. [9]Shanghai Key Laboratory of Maternal Fetal Medicine, Clinical and Translational Research Center of Shanghai First Maternity and Infant Hospital, Frontier Science Center for Stem Cell Research, School of Life Sciences and Technology, Tongji University, Shanghai, China. [10]General Surgery Department, Xiangya Hospital, Central South University, Changsha 410008, China. [11]Shanghai Institute of Immunology, Department of Immunology and Microbiology, Shanghai JiaoTong University School of Medicine, Shanghai, China. [12]Hunan key laboratory of aging biology, Xiangya Hospital, Central South University, Changsha, China. [13]These authors contributed equally: Ming Wen, Yanfang Qiu. ✉email: lunquansun@csu.edu.cn; rongtan@csu.edu.cn

Received: 30 April 2024 Revised: 17 October 2024 Accepted: 23 October 2024
Published online: 8 November 2024

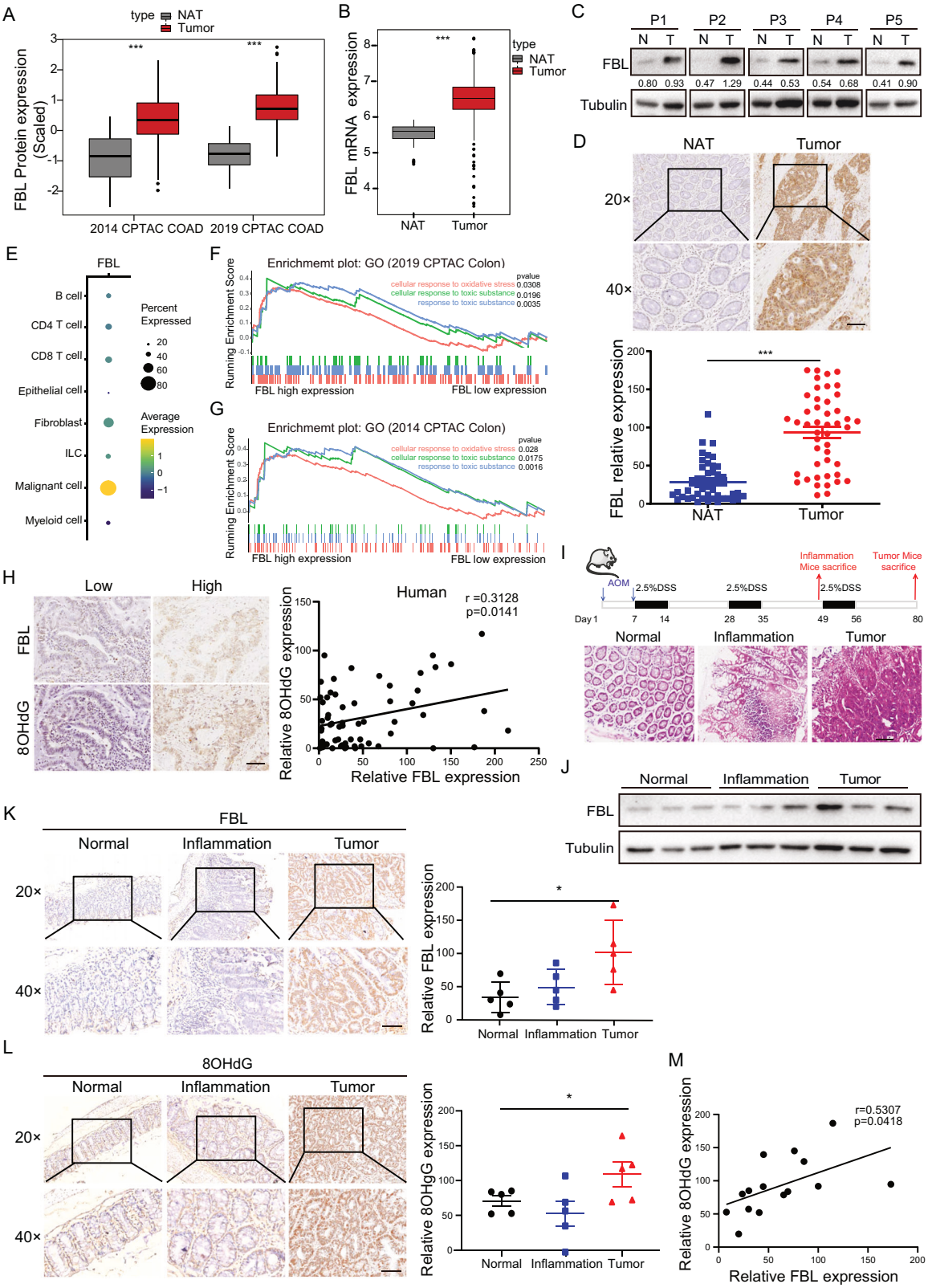


response to various stresses [6, 7]. The high expression of these PARP substrates in cancers, along with their involvement in tumorigenesis pathways, suggests a potential strategy of combining PARP inhibition with other therapeutic approaches.

Increasing evidence suggests that certain tumor-associated genes have distinct functions in physiological processes while also exerting unexpected roles under stress conditions [8, 9]. The high expression of these genes emerges as a new source of mutagenesis and is closely associated with carcinogenesis or therapy resistance [10–12]. Fibrillarin (FBL) is a nucleolar methyltransferase dedicated to RNA processing and ribosome assembly [13]. Aberrant expression of FBL has been observed in several types of cancers, including breast cancer

**Fig. 1 FBL is highly expressed in colorectal cancer and responds to oxidative damage. A** The protein expression of FBL in tumors and NATs analysed in 2019 and 2014 CPTAC COAD databases. NATs, non-cancerous adjacent tissue. (***$p < 0.001$, Wilcoxon rank-sum test). **B** The mRNA level of FBL in tumors and NATs analysed in TCGA-COAD project. (***$p < 0.001$, Wilcoxon rank-sum test). **C** Immunoblotting analysis of FBL protein level in T (tumor) samples and paired N (non-cancerous adjacent tissue) from CRC patients. **D** Immunohistochemical stains of FBL in tumor samples and paired NATs from CRC patients. Representative images of NAT and tumor sample (up) and Quantification of FBL expression (down) were shown. (*$p < 0.05$, **$p < 0.01$, ***$p < 0.001$, error bar = ±SEM, $n = 46$, scale bar =100 μm). **E** Bubble heatmap showing the expression of FBL in each Smart-seq2 cell type of CRC single cell databases (GSE146771). Dot size indicates the percentage of expressed cells, colored by average expression levels. **F** GSEA pathway analysis of proteins enriched in patients with FBL high expression and in patients with FBL low expression in 2019 CPTAC COAD databases. **G** GSEA pathway analysis of proteins enriched in patients with FBL high expression and in patients with FBL low expression in 2014 CPTAC COAD databases. **H** Representative image (left) and Pearson correlation analysis (right) of immunohistochemical stains of FBL and 8-OHdG in 61 CRC patients' tumors. (*$p < 0.05$, error bar = ±SEM, scale bar =100 μm). **I** Schematic diagram of colitis-associated carcinoma C57 mouse model induced by AOM/DSS. The HE staining of normal, inflammatory and tumor intestinal tissues in mice sacrificed as indicated after induction. **J** Immunoblotting analysis of FBL protein levels in normal, inflammatory and tumor intestinal tissues of mice. **K** Representative images (left) and quantification (right) of immunohistochemical stains of FBL in normal, inflammation and tumor intestinal tissues of mice. (*$p < 0.05$, error bar = ±SEM, $n = 5$, scale bar =100 μm). **L** Representative images (left) and quantification (right) of immunohistochemical stains of 8-OHdG in normal, inflammation and tumor intestinal tissues of mice. (*$p < 0.05$, error bar = ±SEM, $n = 5$, scale bar =100 μm). **M** Pearson correlation of FBL and 8-OHdG staining in normal, inflammation and tumor intestinal tissues of mice.

and prostate cancer [14, 15]. Meanwhile, the highly conserved structure of FBL across species and its function in fundamental cellular physiological processes suggest an essential role for FBL, making it a challenging target for drug development. In our study, we reveal that FBL is highly expressed in colorectal tumors and correlated with increased oxidative stress. We further discovered that FBL is directly recruited to DNA damage foci regulated by PARP1 and counteracts oxidative stresses. The DNA damage-accumulated FBL serves as a central hub to favor DNA oxidative damage repair via short-patched base excision repair (BER). Overall, our study identified novel role of FBL in oxidative stress in CRC. More importantly, we demonstrated that low-dose radiotherapy in combination with a PARP inhibitor could be a promising therapeutic strategy for CRC tumors with high expression of FBL.

## RESULTS

### FBL is highly expressed in colorectal cancer and responds to oxidative damage

By analyzing two colorectal cancer databases [16, 17], we discovered that FBL was highly expressed in tumor tissues compared to normal tissues at both the proteomic and mRNA levels (Fig. 1A, B). To verify FBL expression in human CRC, we collected tumor tissues and paired normal tissues adjacent to tumors (NATs) from 46 patients. Consistent with the analysis, FBL expression was elevated in tumor samples compared to NATs, as confirmed by both immunoblotting (Fig. 1C) and immunohistochemical (IHC) staining (Fig. 1D). In addition, we observed that FBL expression was predominantly enriched in tumor sites rather than stromal sites. The scRNA-seq analyses for colorectal cancer further validated that FBL was highly enriched in malignant cells compared to other cell clusters, highlighting the significant roles of FBL in tumor cells [18] (Fig. 1E).

To further investigate the functional involvement of FBL in colorectal tumors, we analyzed FBL-involved pathway enrichments in three proteomic colorectal cancer databases [16, 17, 19]. Interestingly, we observed, for the first time, that the expression of FBL positively correlated with toxic substrates and oxidative stress (Fig. 1F, G, Fig. S1A). Oxidative stresses are known to attack genomic guanine, leading to the formation of 8-hydroxy-2′-deoxyguanosine (8-OHdG) or 8-oxo-7,8-dihydro-2′-deoxyguanosine (8-oxodG), thereby causing oxidative DNA damage. To explore the possible correlations of FBL with oxidative DNA damage, we stained 8-OHdG and FBL in patient tumor samples. Our results demonstrated a positive correlation between FBL expression and 8-OHdG levels (Fig. 1H). To further investigate the association of FBL with oxidative DNA damage and tumorigenesis, we established an azoxymethane/dextran sulfate sodium (AOM/DSS) colitis-associated carcinoma murine model, which recapitulates inflammatory colorectal cancer, and validated pathogenic tissues through HE staining (Fig. 1I). We detected the protein level of FBL in normal, inflammatory, and tumor intestinal tissues and found that FBL expression gradually increased concomitantly with the accumulation of toxic agents, ultimately exhibiting the highest expression in tumors, as demonstrated by both immunoblotting and IHC staining (Fig. 1J, K). Furthermore, we stained for 8-hydroxyguanosine (8-OHdG) in normal, inflammatory, and tumor tissues from the AOM/DSS mouse model. We observed that the level of 8-OHdG increased during tumor development and that FBL expression positively correlated with 8-OHdG staining (Fig. 1L, M). Thus, our data provide evidence that the expression of FBL increases concomitantly with oxidative stresses and is associated with oxidative DNA damage.

### FBL acts as a critical factor in oxidative DNA damage repair and is directly recruited to DNA damage sites

To elucidate the impact of FBL on oxidative damage, we treated FBL-overexpressing colorectal cancer cells with oxidative stresses and observed that cells with FBL overexpression were more resistant to hydrogen peroxide ($H_2O_2$) or KBrO3-induced oxidative damage (Fig. 2A, B, Fig. S2A). In contrast, either RKO or SW480 cells with FBL knockdown were hypersensitive to oxidative damage (Fig. 2C, D, Fig. S2B–E). To further investigate the direct impact of FBL on oxidative stress-induced DNA damage, we performed alkaline comet assays, where the tail length reflects the level of DNA breaks. The results revealed reduced DNA breaks in FBL-overexpressing cells (Fig. 2E) and, conversely, exacerbated breaks in FBL knockdown cells under $H_2O_2$ treatment (Fig. 2F).

To decipher the role of FBL in DNA damage repair, we conducted laser microirradiation to generate localized DNA damage in U2OS cells and then visualized FBL accumulation. Live-cell imaging demonstrated that EGFP-tagged FBL was recruited to the sites of laser-induced DNA damage immediately after microirradiation in the nucleoplasm (Fig. 2G). Analyzing the FBL structure, we observed two main domains: the N-terminal domain and the methyltransferase domain. The N-terminal domain, known as the GAR domain, was defined as a disordered region enriched in arginine and lysine. The methyltransferase domain consisted of the RNA-binding (RB) domain and the α-helix domain (Fig. 2H). To determine which domain is needed for the DNA damage response of FBL, we then constructed three truncations: FBL truncated GAR (ΔGAR), RB (ΔRB) or α-helix domain (Δα-helix). Intriguingly, the damage response of the different truncations showed that GAR was a domain required for DNA damage recruitment of FBL, as evidenced by the fact that FBL-truncated GAR completely lost laser microirradiation-induced accumulation. The other truncations of FBL maintained the DNA damage response (Fig. 2I, J).

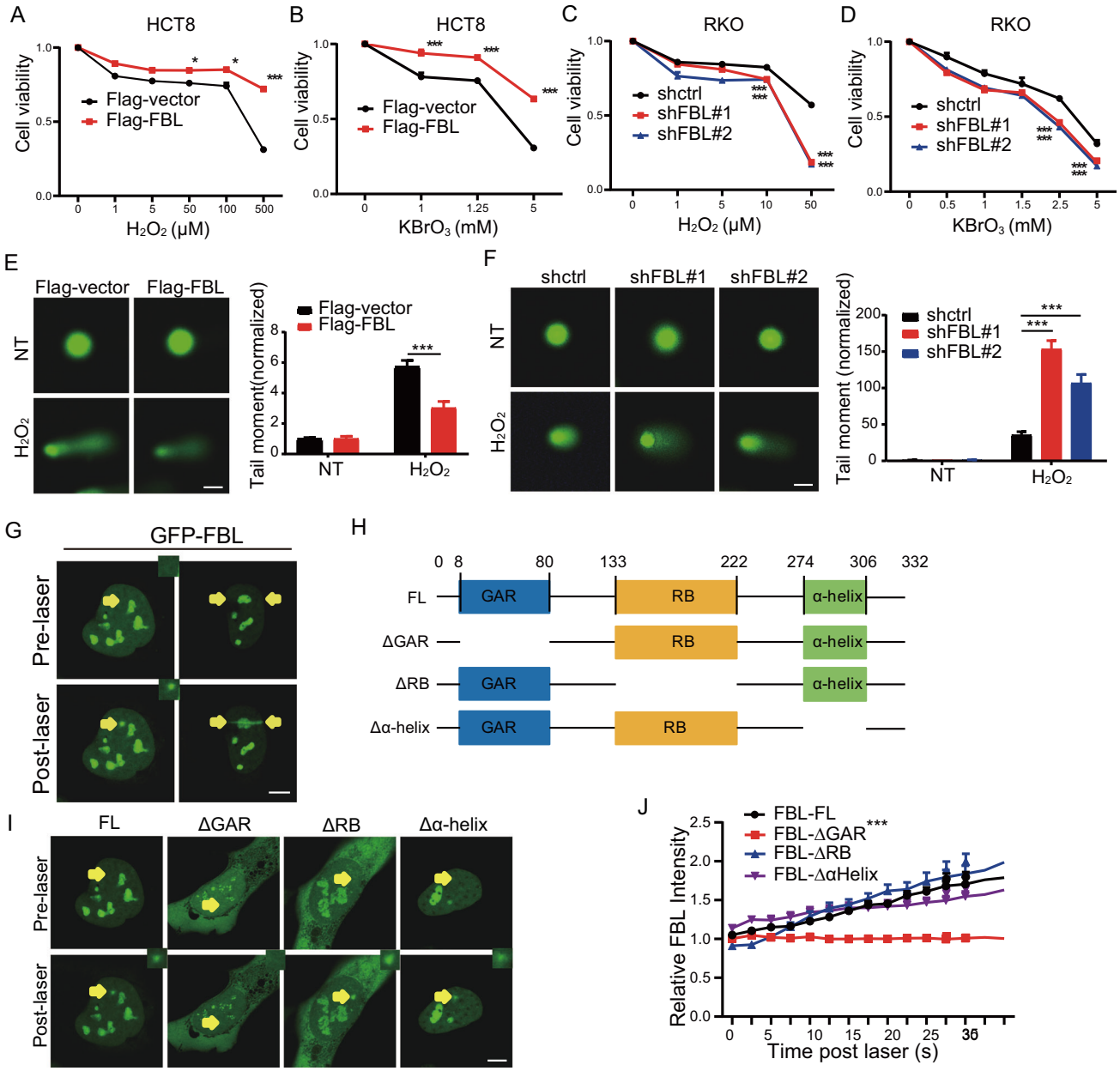


**Fig. 2 FBL acts as a critical factor in oxidative DNA damage repair and is directly recruited to DNA damage sites.** Cell viability of HCT8 cell lines stably overexpressing Flag or Flag-FBL. The cells were exposed to $H_2O_2$ **A** or $KBrO_3$ **B** at concentrations as indicated for 48 h and then analysed by CCK8 assay. (*$p < 0.05$, ***$p < 0.001$, error bar = ±SEM, $n = 5$). Cell viability of RKO cell lines stably expressing control shRNA (shctrl) or FBL-targeted shRNA (shFBL). The cells were exposed to $H_2O_2$ **C** or $KBrO_3$ **D** at concentrations as indicated for 48 h and then analysed by CCK8 assay. (***$p < 0.001$, error bar = ±SEM, $n = 5$). **E** Alkaline comet assays for HCT8 cell lines stably overexpressing Flag and Flag-FBL. Cells were treated with 1 mM $H_2O_2$ for 20 min and then harvested 1 h after recovery. Representative images (left) and quantification (right) were shown. (***$p < 0.001$, error bar = ±SEM, $n = 20–50$, scale bar =20 μm). **F** Alkaline comet assays for RKO cell lines stably expressing shctrl, shFBL #1 or shFBL#2. Representative images (left) and quantification (right) were shown. (***$p < 0.001$, error bar = ±SEM, $n = 20–50$, scale bar =20 μm). **G** The recruitments of EGFP-FBL to the DNA damage sites induced by 405 nm microirradiation in U2OS cells. Yellow arrows represent laser points/lines induced by 405 nm laser. (scale bar =2.5 μm). **H** Schematic representation of the FBL truncations (left). FL, FBL Full-length; ΔGAR, truncated mutants lacked residues 8–80 aminol acid (aa) for glycine and arginine rich (GAR) domian; ΔRB, mutant lacked residues 133–222 aa for RNA binding (RB) domain; Δα-helical, mutant lacked residues 274-306 aa. **I** The recruitments of EGFP-FBL-FL, EGFP-FBL ΔGAR, EGFP-FBL ΔRB, EGFP-FBL Δα-helix to the DNA damage sites induced by 405 nm microirradiation in U2OS cells. (scale bar =2.5 μm,). **J** The quantification of time-lapse recruitments of EGFP-FBL FL and truncations to DNA damage sites induced by 405 nm microirradiation in U2OS (right). (***$p < 0.001$, error bar =±SEM, $n = 10–15$ cells).

## PARP1 serves as the upstream regulator of the DNA damage response of FBL

The initiation of DNA damage repair and pathway choice relies on the mediation of a series of early and upstream regulators, including members of the phosphatidylinositol 3 kinase (PI3K)-like kinases (PIKK) family, such as ataxia-telangiectasia mutated (ATM), Rad3-related protein (ATR), DNA-dependent protein kinase (DNA-PK), and DNA damage sensor poly-(ADP-ribose) polymerase 1 (PARP1). To explore the upstream factors that might regulate FBL-related DNA damage repair, we pretreated the cells with ATM, ATR, DNA-PK or PARP

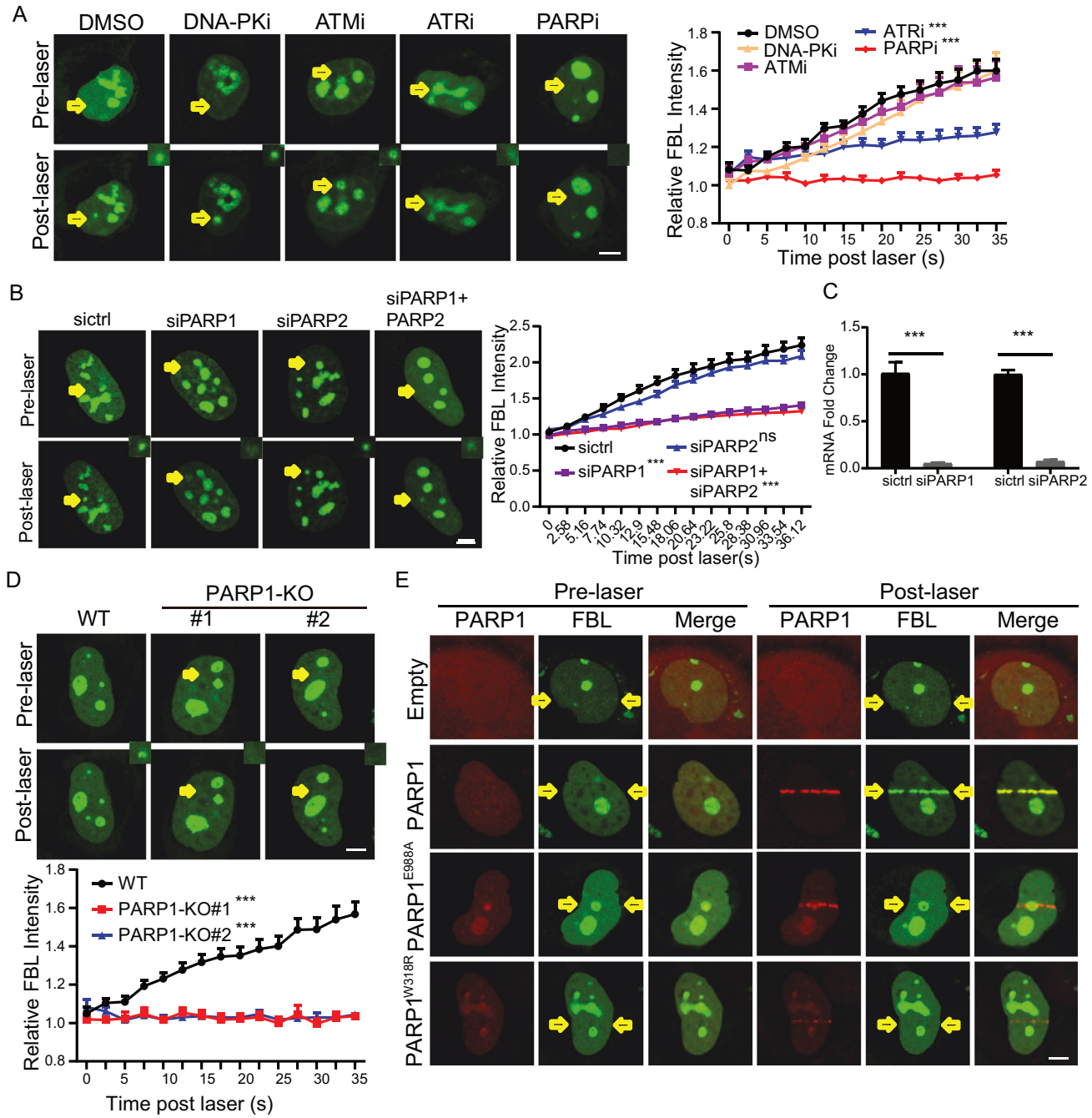


**Fig. 3 PARP1 serves as the upstream regulator of the DNA damage response of FBL. A** The representative images (left) and quantification of normalized fluorescent intensity (right) of EGFP-FBL recruited to DNA damage sites induced by 405 nm microirradiation in U2OS cells pretreated with DMSO (control) or inhibitors as indicated. ATMi: ATM inhibitor KU55933 (10 μM for 1 h), ATRi: ATR inhibitor AZD6738 (1 μM for 24 h); DNA-PKi: DNA-PK inhibitor PI103 (2.5 μM for 24 h); PARPi: PARP inhibitor Olaparib (5 μM for 24 h). (***$p < 0.001$, error bar =±SEM, $n = 10–15$ cells, scale bar =2.5 μm). **B** The recruitments of EGFP-FBL to the DNA damage sites induced by microirradiated in U2OS transfected with siRNA as indicated (left). Intensity dynamics of EGFP-FBL recruited to DNA damage sites induced by 405 nm microirradiation were shown (right, ***$p < 0.001$, error bar =±SEM, $n = 10–15$ cells, scale bar =2.5 μm). **C** The mRNA expression levels of PARP1 and PARP2 in cells transfected with non-targeting siRNA (sictrl), siRNA targeting at PARP1 (siPARP1) and PARP2 (siPARP2) analysed by qPCR were shown (***$p < 0.001$, error bar = ±SEM, $n = 3$). **D** The representative images (top) and the intensity dynamic analysis (bottom) of EGFP-FBL recruited to the DNA damage sites induced by 405 nm microirradiation in HeLa cells (WT) or PARP1 knockout (KO) HeLa cells. (***$p < 0.001$, error bar = ±SEM, $n = 10–15$ cells, scale bar =2.5 μm). **E** The representative images of EGFP-FBL recruited to the DNA damage sites induced by 405 nm microirradiation in PARP1 KO HeLa cells co-transfected EGFP-FBL with RFP-empty, RFP-PARP1, RFP-PARP1$^{E988A}$ or RFP-PARP1$^{W318R}$ respectively. (scale bar =2.5 μm).

inhibitors individually before laser microirradiation. Interestingly, the DNA damage response of FBL was completely abolished by a PARP inhibitor (olaparib) and partially inhibited by ATR inhibitors but remained unchanged under treatment with other inhibitors in both U2OS and RKO colon cancer cell (Fig. 3A, Fig. S3A). Olaparib targets both PARP1 and PARP2. To further characterize which PARP family members are necessary for the DNA damage response of FBL, we investigated the recruitment of FBL after laser microirradiation in

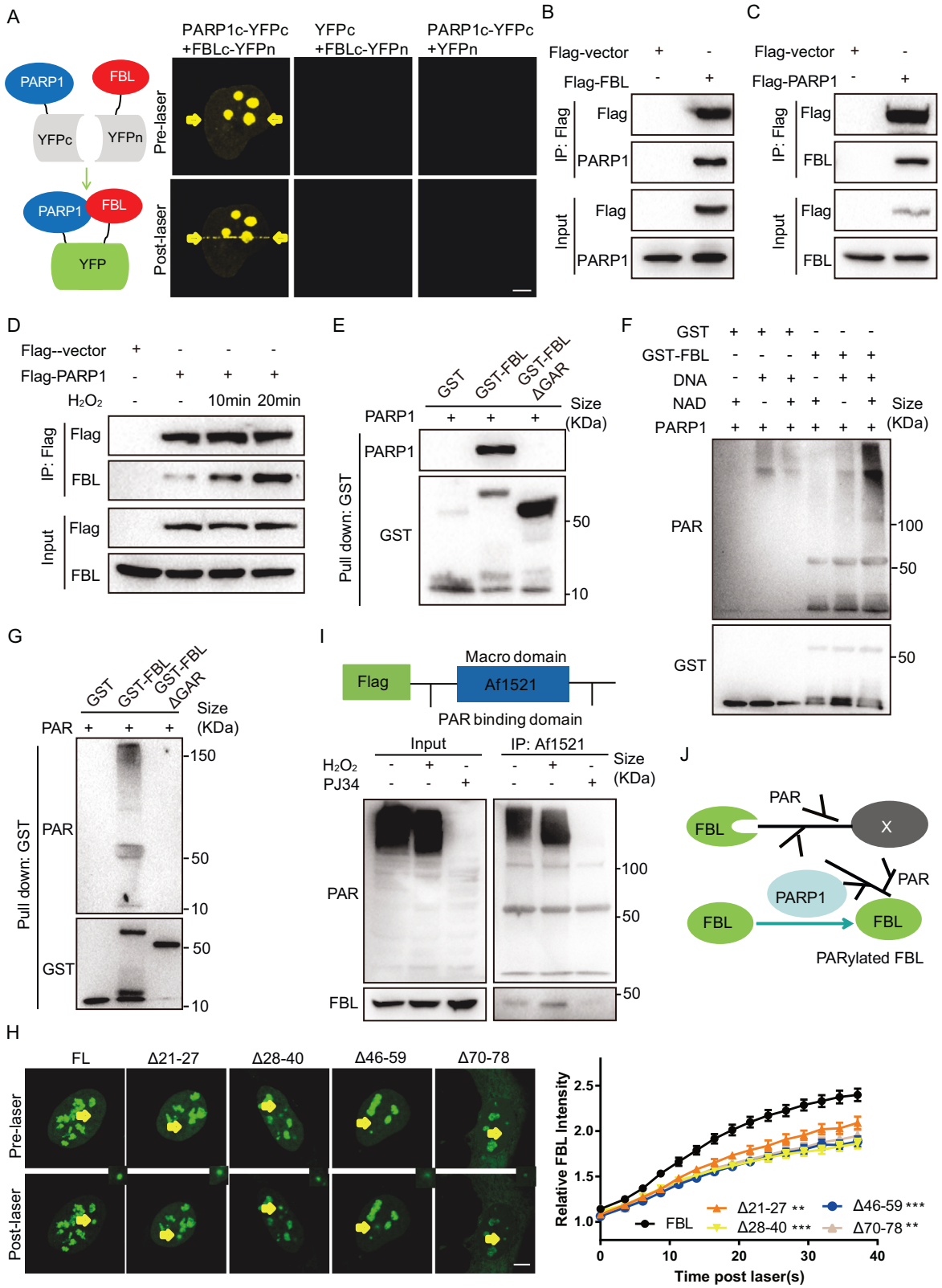


PARP1 or PARP2 knockdown cells or knockout cells. The results suggested that depletion of PARP1, but not PARP2, significantly reduced the accumulation of FBL at DNA damage sites (Fig. 3B–D, Fig. S3B). Meanwhile, we demonstrated that endogenous FBL accumulated at damage sites following microirradiation-induced damage. This accumulation was further prevented by either a PARP inhibitor or PARP1 knockdown (Fig. S3C). In addition, recruitment of FBL was recovered in PARP1 -/- cells rescued by the PARP1 WT, but not PARP1 kinase dead mutants, E988A or W318R (Fig. 3E). Furthermore, olaparib or PARP1 knockdown did not affect the expression of FBL (Fig. S3D). These data collectively suggest that PARP1 serves as the upstream regulator of the DNA damage response of FBL.

**Fig. 4 FBL interacts with PARP1 through the GAR domain and is PARylated by PARP1. A** Schematic illustration of bimolecular fluorescence complementation (BiFC) assay (left). FBL was fused to the N-terminal of YFP (YFPn) (FBL-cYFPn). PARP1 was fused to the C-terminal of YFP (YFPc) (PARP1-cYFPc). The images of YFP signal at DNA damage sites induced by 405 nm microirradiation in cells co-transfected FBL-cYFPn with YFPn or PARP-cYFPc, or PARP-cYFPc with YFPn (right) in U2OS cells. **B** Co-immunoprecipitation of Flag-SBP-FBL with endogenous PARP1 in HEK293T cells. **C** Co-immunoprecipitation of Flag-SBP-PARP1 with endogenous FBL in HEK293T cells. **D** Co-immunoprecipitation of Flag-SBP-PARP1 with endogenous FBL in HEK293T cells with or without 1 mM $H_2O_2$ treatment for 10 min or 20 min as indicated. **E** In vitro binding assay for GST-FBL with PARP1. Bacterial purified GST, GST-FBL and GST-FBL ΔGAR proteins were incubated with PARP1 protein overnight and then precipitated with GST sepharose beads. **F** In vitro binding assay for GST-FBL with PAR polymer. Bacterial purified GST, GST-FBL and GST-FBL ΔGAR proteins were incubated with PAR polymer overnight and then precipitated with GST sepharose beads. **G** In vitro PARylation assay for GST-FBL by PARP1. **H** The recruitments of EGFP-FBL-FL, EGFP-FBLΔ21-27 aa (amino acids), EGFP-FBL Δ28-40 aa, EGFP-FBL Δ46-59 aa, EGFP-FBLΔ70-78 aa to the DNA damage sites induced by 405 nm microirradiation in U2OS cells(left). (scale bar =2.5 μm). The quantification of time-lapse recruitments of EGFP-FBL FL and truncations to DNA damage sites induced by 405 nm microirradiation in U2OS (right). (***$p < 0.001$, error bar =±SEM, $n = 10–15$ cells). **I** The schematic illustration for constructing Flag-SBP-Af1521 (Macro domain) (top). The immunoblotting analysis of FBL were preformed in Flag-SBP-Af1521 precipitants in HEK293T cells with or without 2 mM $H_2O_2$ treatment for 20 min (bottom). The PJ34 (40 mM) was preincubated for 1.5 h before $H_2O_2$ treatment. **J** The schematic illustration of FBL PARylated by PARP1 or recognizing PARylated protein.

## FBL could either be PARylated by PARP1 or recognize PARylated proteins

To determine how PARP1 regulates FBL, we first employed a bimolecular fluorescence complementation (BiFC) assay to detect the interaction of PARP1 and FBL in live cells [20]. PARP1 and FBL were fused with the N-terminal (YFPn, residues 1–155) and C-terminal (YFPc, residues 156–239) fragments of the Venus variant of yellow fluorescent protein (YFP), respectively (Fig. 4A). A strong yellow fluorescent signal was observed at laser-induced DNA damage sites in both U2OS and RKO CRC cells transfected with PARP1-YFPc and FBL-YFPn, confirming their interaction. However, no fluorescence was observed in cells with the fusion protein alone (Fig. 4A, Fig. S4A). Furthermore, we confirmed the interactions between FBL and PARP1 through reciprocal coimmunoprecipitation (Fig. 4B, C). In addition, $H_2O_2$ treatment greatly enhanced the interaction of FBL and PARP1 (Fig. 4D). We previously demonstrated that the GAR domain is crucial for the DNA damage response of FBL. We next investigated whether the interaction of FBL and PARP1 relies on the GAR domain. Using an in vitro pull-down assay, we purified GST-tagged FBL (GST-FBL) or GST-tagged FBL truncated GAR (GST-ΔGAR) proteins from bacteria and incubated them with the PARP1 protein individually. The results showed that only GST-FBL interacted with and pulled down PARP1, while GST-ΔGAR failed to interact (Fig. 4E), indicating that FBL interacts with PARP1 directly through the GAR domain.

PARP1 is activated by DNA lesions and plays a crucial role as an early sensor for DNA damage. Activated PARP1 subsequently PARylates numerous DNA damage response (DDR)-related proteins, amplifying repair cascades [21–23]. The PARP1-dependent DNA damage response of FBL suggests two possibilities: FBL may act as a PARylated substrate catalyzed by PARP1, or FBL may recognize PARylated proteins. To explore these possibilities, we first examined the in vitro PARylation of FBL. We observed that FBL was PARylated by PARP1 only under the condition of complete supplementation of DNA and NAD+ (Fig. 4F), while FBL showed no apparent PARylation under incubation with either DNA or NAD+ alone. Consistent with in vitro assay, we observed increased PARylation of pull-down FBL after PARP1 overexpression in response to $H_2O_2$ treatment in the SW480 CRC cell line (Fig. S4B). We then investigated the interaction of FBL with PARylation and found that FBL directly bound to PAR through its GAR domain in vitro (Fig. 4G). To demonstrate whether the recognition of PAR by FBL or PARylated FBL occurs in vivo, we employed two PAR binding macro domains, PBZ (PAR-binding zinc finger) and the AF1521 macrodomain, which recognize and bind PAR with high affinity [24–26]. We fused PBZ and FBL with YFPc and YFPn (PBZ-YFPc and FBL-YFPn) and coexpressed them in U2OS cells, observing bright fluorescent signals accumulated at laser-induced DNA damage sites, similar to the observations in Fig. 4A (Fig. S4C). In addition, we fused PBZ with mRuby fluorescent protein (PBZ-mRuby) and coexpressed PBZ-mRuby with PARP1-YFPc and FBL-YFPn. As expected, under laser microirradiation-induced DNA damage, PBZ-mRuby accumulated at the DNA damage site and colocalized with the FBL/PARP1 YFP signal (Fig. S4D). Next, we used another PAR-recognizing domain, Af1521, and performed an Af1521-directed pull-down experiment to obtain extensive PARylated proteins [6]. FBL was detected in Af1521 precipitates (Fig. 4I). Furthermore, the FBL signal was enhanced following $H_2O_2$ treatment and completely abolished under pretreatment with the PARP inhibitor PJ34 (Fig. 4I).

To further explore the PARylation sites, we mutated specific amino acids including Asp, His, Ser, Arg in the GAR domain according to preferential ADP-ribosylation sites for PARP1 [7]. However, none of these mutants completely abolished the DNA damage response of FBL (Fig. S4E, F). We then sequentially deleted several amino acids in the GAR domain and validated the DNA damage response of all mutants. Four mutants with deletions at amino acids Δ21-27, Δ28-40, Δ46-59, and Δ70-78 exhibited attenuated DNA damage response (Fig. 4H, Fig. S4G), indicating that PARP1 regulates the damage response of FBL through the entire GAR domain of FBL or multiple sites. Taken together, these results indicate that FBL could either be PARylated by PARP1 or recognize PARylated proteins (Fig. 4J).

## FBL facilitates short-patched base excision repair pathway

Assuming that oxidative damage repair and subsequent base excision repair (BER) pathways play key roles in repairing oxidative damage, we carried out a BER assay [27] and observed that the repair efficiency within BER pathways was diminished in FBL-knockdown (shFBL) cells compared with control (shctrl) cells (Fig. 5A). However, this reduction was reversed upon reintroduction of FBL into the cells (Fig. 5B).

We then examined the response of key factors involved in processing oxidative DNA damage and the BER pathway to determine the downstream effects of FBL regulation. The results showed that DNA Ligase III (Lig III), a factor in the short-patch BER pathway, accumulated rapidly in cells supplemented with FBL. Conversely, the damage response of factors involved in the long-patch BER pathway, such as flap structure-specific endonuclease 1 (FEN1), proliferating cell nuclear antigen (PCNA), and Replication Factor C Subunit 1 (RFC1), was quicker to disassociate in FBL-supplemented cells compared to FBL-knockdown cells (Fig. 5C–E, Fig. S5A, B). However, factors associated with the short-patch BER pathway, like X-ray repair cross complement 1 (XRCC1) and polymerase β (Polβ), did not exhibit altered DNA damage response (Fig. S5C, D).

Furthermore, we observed rapid disassociation of 8-oxoguanine DNA glycosylase 1 (OGG1) in cells supplemented with FBL, while OGG1 was retained at damage sites in FBL-deficient cells or cells rescued only by FBL GAR truncation (Fig. S5E). The response of apurinic/apyrimidinic endodeoxyribonuclease 1 (APEX1) and Nth-like DNA glycosylase 1 (NTHL1) did not show significant changes

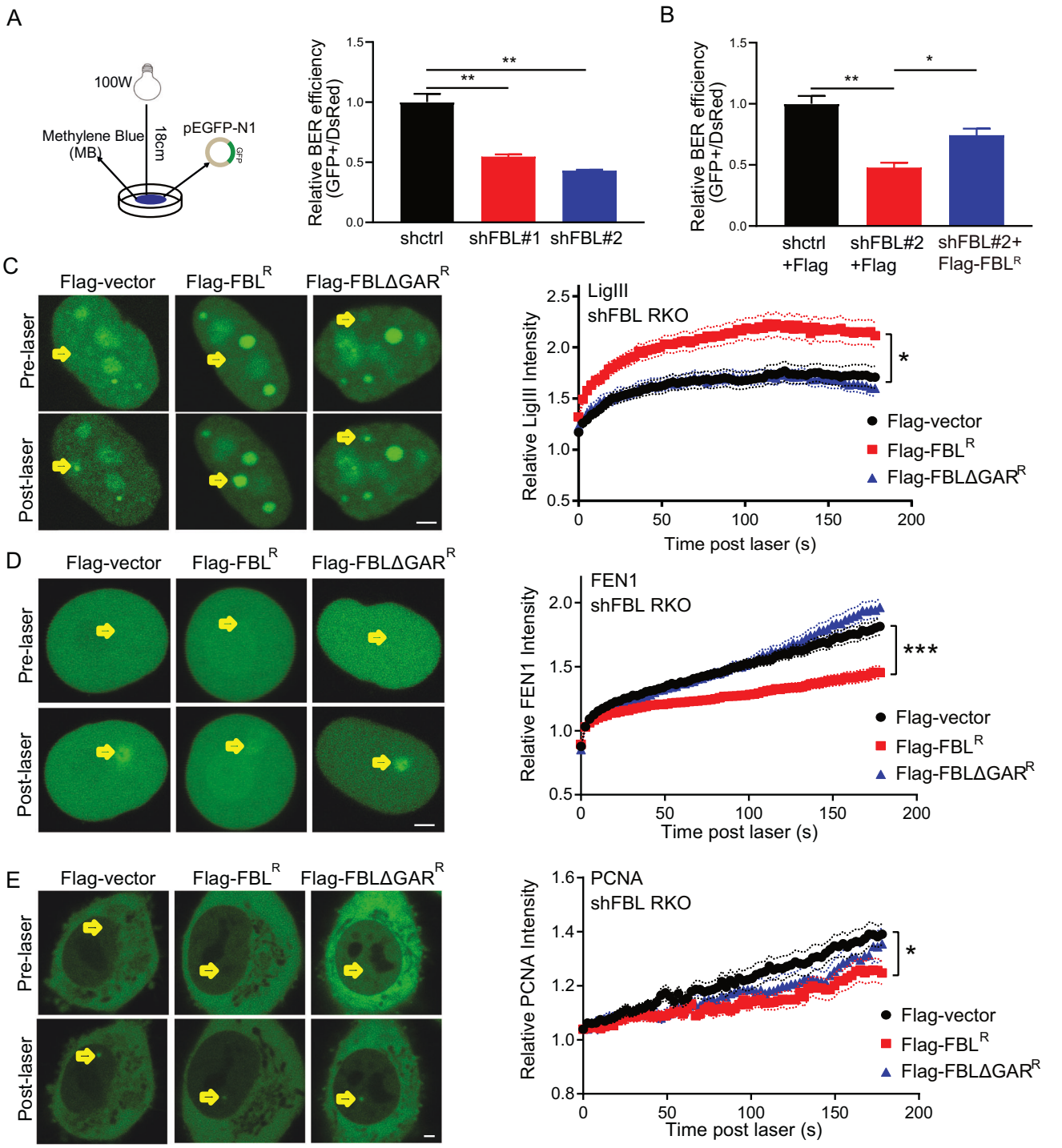


**Fig. 5 FBL facilitates short-patched base excision repair pathway. A** The schematic illustration of BER efficiency assay (left). The BER efficiency assay (the ratio of GFP+ cells to DsRed+ cells analysed by FACS after 48 h transfection) in shctrl or shFBL (#1, #2) RKO cell lines (right) (**$p < 0.01$, error bar = ±SEM, $n = 3$). **B** The BER assay in shctrl, shFBL RKO cells stably expressing Flag empty vectors or shFBL RKO cells rescued by shFBL resistant Flag-FBL$^R$. (*$p < 0.05$, **$p < 0.01$, error bar = ±SEM, $n = 3$). The recruitments (left) and intensity analyses (right) of EGFP-Lig III **C** EGFP-FEN1 **D** and EGFP-PCNA **E** recruited to the DNA damage sites induced by 405 nm microirradiation in shFBL#2 RKO cells stably expressing Flag-empty, Flag-FBL$^R$ or Flag-FBLΔGAR $^R$, respectively. (*$p < 0.05$, **$p < 0.01$, error bar = ±SEM, $n = 10$–15 cells, scale bar = 2.5 μm).

between FBL-knockdown cells and FBL-rescued cells (Fig. S5F–G). Additionally, we observed a negative correlation between FBL expression and single-nucleotide polymorphisms (SNPs) in the TCGA (The Cancer Genome Atlas Program) CRC database (Fig. S5H). These findings collectively suggest that FBL facilitates short-patch BER while suppressing long-patch BER.

**Elevated expression of FBL reduces the accumulation of DNA breaks during oxidative stress**

The balance between DNA damage and repair capacity is critical for maintaining genome integrity, as excessive oxidative damage beyond repair capacity can result in the formation of double-strand DNA breaks. Phosphorylation of the histone variant H2AX

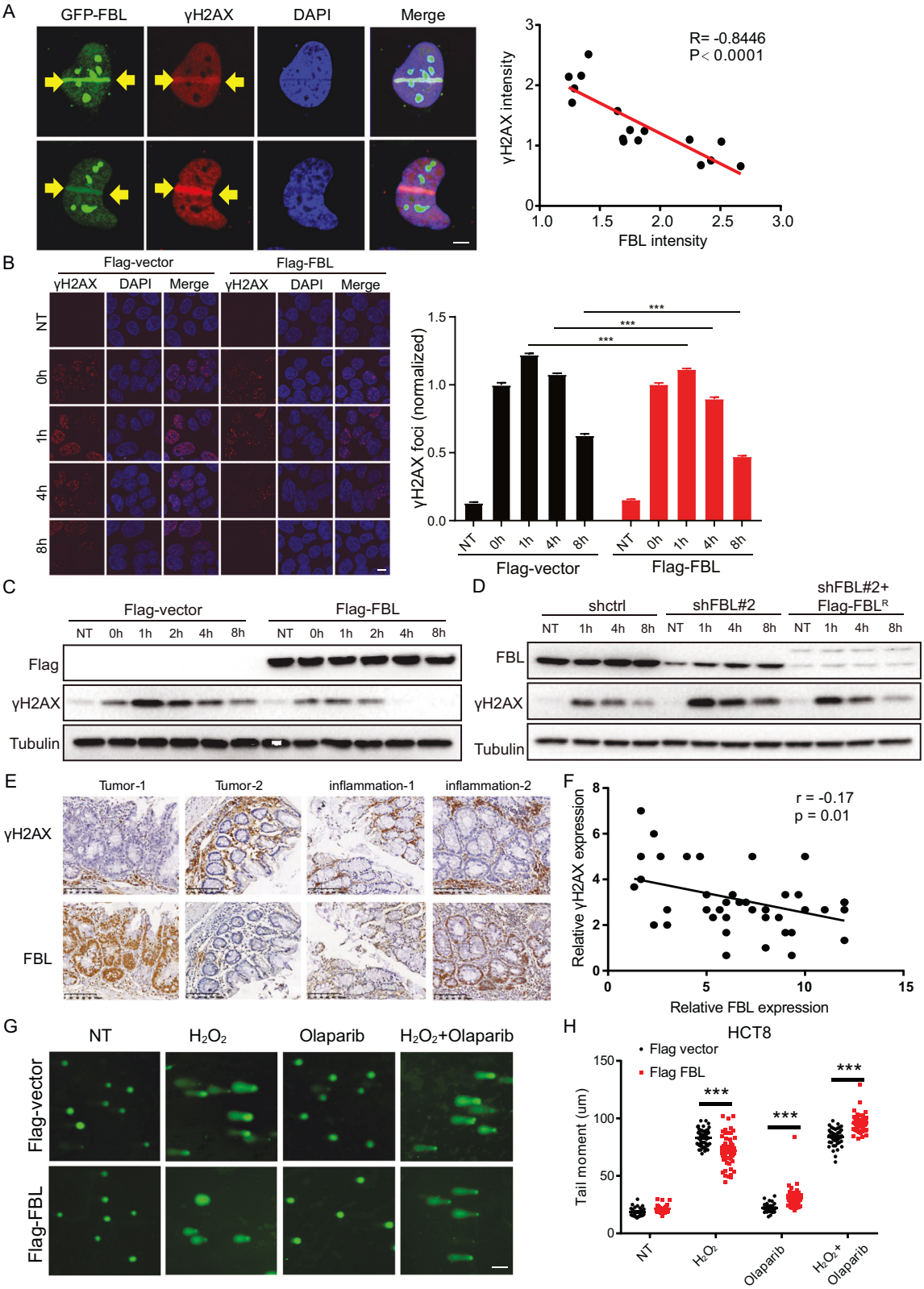


at site Ser 140, known as γH2AX, serves as an early indicator of double-strand DNA damage [28]. Utilizing laser microirradiation-induced DNA damage, we found an intriguing negative correlation between the intensity of exogenous or endogenous FBL and γH2AX in U2OS and HCT8 cell lines (Fig. 6A, Fig. S6A). To evaluate the repair dynamic, we then examined the kinetics of γH2AX in cells with either overexpressed or depleted levels of FBL. Remarkably, FBL overexpression led to the rapid disappearance of γH2AX foci following oxidative damage (Fig. 6B). A similar result was obtained by γH2AX western blotting. (Fig. 6C). Conversely, in

**Fig. 6 High expression of FBL reduces the level of DNA breaks under oxidative stress. A** Representative images (left) and Pearson correlation (right) of the fluorescence intensity of EGFP-FBL (green) merged with immunofluorescent stain of γH2AX (red) in U2OS cells immediately after microirradiation. (scale bar =2.5 μm). **B** The percentage of HCT8 cell lines stably overexpressing Flag and Flag-FBL with positive γH2AX foci. The cells were treated with 1 mM $H_2O_2$ for 20 min and then recovery and collected at indicated time points. Cells with ≥5 foci were defined as positive cells. The fold changes were calculated by normalized the time point collected to the time points immediately after drug withdrawal (0 h). (***$p < 0.001$, error bar = ±SEM, scale bar =10 μm, $n \geq 300$ cells). **C** Immunoblotting analysis of γH2AX in HCT8 cell lines stably expressing Flag or Flag-FBL. **D** Immunoblotting analysis of γH2AX in shctrl, shFBL knockdown RKO cell lines or shFBL knockdown cell lines rescued by Flag-FBL$^R$. **E**, **F** Representative image **E** and Pearson correlation **F** of immunohistochemical stains of paired γH2AX and FBL in inflammation and tumor intestinal tissues of mice. (scale bar =100 μm). **G**, **H** Alkaline comet assays for HCT8 cell lines stably overexpressing Flag and Flag-FBL. Cells were treated with 1 mM $H_2O_2$ for 20 min and then harvested 1 h after recovery or 50uM olaparib 48 h as indicated. Representative images **G** and quantification **H** were shown. (***$p < 0.001$, error bar = ±SEM, $n > =30$, scale bar =20 μm).

FBL-deficient cells, γH2AX levels remained sustained and gradually declined (Fig. S6B, C), a trend that was reversed upon FBL complementation (Fig. 6D). To validate the relationship between FBL and γH2AX in carcinogenesis, we examined FBL and γH2AX expression in inflammatory and tumor samples from the AOM/DSS colitis-associated carcinoma murine model. Intriguingly, we observed a negative correlation between FBL expression and γH2AX levels during tumorigenesis (Fig. 6E, F), suggesting that FBL plays an indispensable role in preventing DNA double strand breaks.

The discovery of PARP as an upstream regulator of FBL in the DNA damage response opens new possibilities for application of PARP inhibitor (PARPi) in CRC with high FBL expression. PARP inhibitors (PARPis) have been extensively used in cancers with HRD [5], while their potential in colorectal cancers is still under investigation. We assessed the extent of DNA breaks in cells overexpressing FBL under oxidative stress alone or in combination with PARP inhibition. Our results showed a reduction in DNA breaks in FBL-overexpressing cells treated with $H_2O_2$ alone, but an exacerbation of DNA breaks was observed under treatment with both $H_2O_2$ and PARPi (Fig. 6G, H). These findings indicate that high expression of FBL mitigates the extent of DNA breaks induced by oxidative stress. Moreover, inhibiting FBL function through PARP inhibition could exacerbate the DNA damage caused by oxidative stress.

### PARP inhibitor enhances radiotherapy in FBL highly expressed colorectal cancer

Low doses of ionizing radiation (IR) induce cell death through accumulated oxidative damage. We evaluated the impact of treating cancer cells and tumors overexpressing FBL with a PARPi alone or in combination with a low dose of ionizing radiation (IR). The results showed that treatment with IR or olaparib alone modestly reduced the survival of cells expressing either empty vectors or FBL (Fig. 7A, B). However, combining PARPi with IR significantly decreased the viability of FBL-overexpressing cells compared to control cells (Fig. 7A, B). To further investigate this therapeutic approach in tumors, we established a xenograft mouse model using FBL-overexpressing cells or vector cells (Fig. 7C). Treatment of tumor-bearing mice with IR, olaparib, or the combination of IR with olaparib resulted in slightly reduced tumor growth. Notably, FBL-overexpressing tumors exhibited increased sensitivity to the combination of IR with olaparib compared to the vector group (Fig. 7D–F, Fig. S7A). In addition, immunohistochemical staining of γH2AX in residual tumors indicated a significant increase in DNA damage in FBL high-expressing tumors compared to other groups following combined treatment (Fig. 7G, H, Fig. S7B), highlighting the potential alternative application of PARPi in combination with radiotherapy in FBL high-expressing CRC.

## DISCUSSION

Given the metabolic function of the intestine, elevated levels of oxidative stress emerge as a primary factor contributing to the tumorigenesis of colorectal cancer (CRC). Consequently, tumor cells evolve mechanisms to counteract oxidative stress in order to survive. This adaptation to oxidative stress becomes a crucial determinant in the resistance of tumors to therapies such as radiotherapy. In our study, we discovered that FBL is highly expressed in CRC and positively correlated with oxidative damage. Our findings reveal that FBL is directly recruited to DNA damage sites under the regulation of PARP, playing a central role in counteracting oxidative DNA damage. The accumulation of FBL facilitates DNA damage repair via short-patched repair. Hence, we suggest that combining PARP inhibitors (PARPis) with radiotherapy presents a prospective therapeutic strategy for CRC patients with high FBL expression.

Intracellular oxidative damage originating from metabolic, detoxification, and inflammatory processes serves as a significant driver of CRC evolution. To counteract oxidative stresses, cells have evolved a series of DNA repair pathways to precisely control oxidative DNA damage. Glycosylases recognize oxidized bases and remove them to generate AP (apurinic/apyrimidinic) sites, which are predominantly excised by AP endonucleases and repaired via the base excision repair (BER) pathway. Our investigation revealed a positive correlation between the expression of FBL and oxidative damage in CRC (Fig. 1). Interestingly, we did not observe a significant increase in FBL expression under acute oxidative stress. However, high levels of FBL expression were associated with reduced DNA breaks under oxidative damage conditions. This suggests that FBL may be gradually elevated during chronic and cumulative oxidative stress, playing an essential role in CRC survival by counteracting oxidative stress. In addition, we demonstrated that FBL facilitates BER repair, further implicating its involvement in oxidative damage repair mechanisms. The association of FBL with oxidative damage implies its potential role in radiotherapy resistance. Low-dose radiotherapy induces oxidative damage in cancer cells, leading to cell death, while high doses of radiation may induce double-strand breaks. Genes involved in eliminating oxidative stresses or damage may serve as key factors in inducing resistance to low-dose radiotherapy. Therefore, inhibition of FBL accumulation by PARP1 inhibitor in combination with low-dose radiotherapy could increase the sensitivity of CRC cells to radiation therapy.

PARP1 functions as an early DNA damage sensor, orchestrating a wide array of downstream DNA repair factors through PARylation [22, 23, 29]. The DNA damage response of FBL is regulated by PARP1 (Fig. 3 and Fig. 4). Similar to many DNA repair proteins, PARP1 interacts with FBL and PARylated FBL at its disordered and low-complexity GAR domain. PAR is preferentially seeded at the low-complexity domains (LCDs) of DNA damage proteins, facilitating rapid assembly of these proteins at DNA damage sites through phase-phase separation [30]. While several sequences within the FBL GAR domain, such as Δ28-40, Δ46-59 and Δ70-78, are crucial for PARP1-mediated modification, the specific PARylation site of FBL remains undefined. Interestingly, minor truncations or point mutations at the N-terminus fail to completely block the DNA damage response of FBL, suggesting complexity in its regulation. Additionally, recent proteomic analyses have identified a plethora of PARylated proteins in

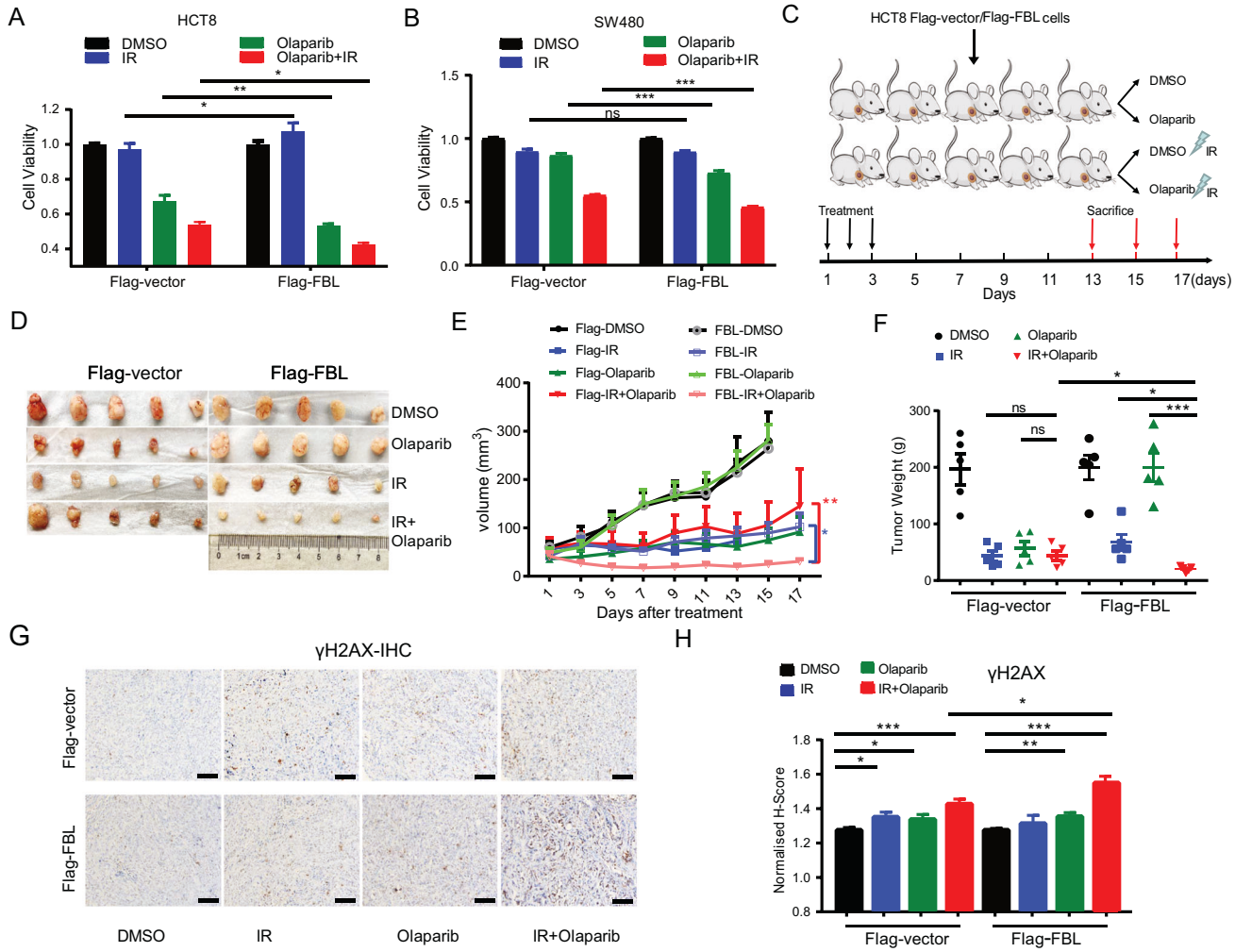


**Fig. 7 PARP inhibitor enhances radiotherapy in FBL highly expressed colorectal cancer. A** Cell viability of HCT8 cell lines stably overexpressing empty vector Flag or Flag-FBL. The cells were exposed to 10 μM olaparib or 2 Gy IR as indicated and then analysed by CCK8 assay. (*$p < 0.05$, ***$p < 0.001$, error bar = ±SEM, $n = 6$). **B** Cell viability of SW480 cell lines stably overexpressing empty vector Flag or Flag-FBL. The cells were exposed to 10 μM olaparib or 2 Gy IR as indicated and then analysed by CCK8 assay. (*$p < 0.05$, ***$p < 0.001$, error bar = ±SEM, $n = 6$). **C** Schematic diagram of nude mice implant model and treatment schedule. Mice of HCT8 Flag/ Flag-FBL cell line were randomized to 4 groups as indicated ($n = 5$): (1) the vehicle group (10%DMSO / 30%PEG300 / saline solution for 3 days by intraperitoneal injection); (2) the olaparib group (olaparib (50 mg/kg/day) for 3 days by intraperitoneal injection); (3) the irradiation group (10%DMSO / 30%PEG300 / saline solution for 3 days by intraperitoneal injection, tumor-localized irradiation (2 Gy) given 1 h after the dose of DMSO); (4) the combination group (olaparib (50 mg/kg/day) for 3 days by intraperitoneal injection, tumor lacalized irradiation (2 Gy) given 1 h after the dose of olaparib). **D** Tumors isolated from individual mice. **E** Growth curve of xenograft tumors derived from indicated group of Flag and Flag-FBL HCT8 cells. Tumor volumes were measured at indicate time points. ($n = 5$, Error bars represent SEM, *$p < 0.05$, **$p < 0.01$, ***$p < 0.001$, two-sided, unpaired *t*-test). **F** The tumor weight measured at the end of the treatments (n = 5, Error bars represent SEM, *$p < 0.05$, *** $P < 0.001$, two-sided, unpaired *t*-test). **G** Representative image of immunohistochemical (IHC) staining for DNA damage maker γH2AX in tumor samples derived from indicated xenografts in nude mice. Scale bar, 100 μm. **H** Quantitation of the normalized histological score (H score) of γH2AX with three individual view for each tumor in different treatment groups as indicated.

response to various stresses [6, 7]. We observed significant enrichment of FBL in PARylated precipitates under hydrogen peroxide ($H_2O_2$) treatment, further affirming its modification by PARP. Intriguingly, FBL also exhibits the ability to recognize PARylated proteins. The involvement of PARP in FBL-mediated DNA damage repair suggests a potential role for PARP inhibitors in tumors with high expression levels of FBL. Although PARP inhibitors have shown efficacy in treating HR-deficient ovarian and breast cancers [31], their clinical outcomes in CRC have been less satisfactory. We propose that CRC patients with high FBL expression levels could benefit from treatment with PARP inhibitors in combination with radiotherapy. This combinatorial approach may enhance therapeutic efficacy by targeting FBL-mediated DNA repair pathways, thus sensitizing CRC cells to radiotherapy-induced damage. However, the optimal radiation dose for this combinatorial treatment in vivo requires further clinical investigation and trials.

FBL serves a fundamental role in RNA processing during transcription and ribosomal synthesis within nucleoli [32, 33]. As reported, FBL can transcriptionally increase BRCA1 expression, contributing to cell resistance against DNA crosslinking agents [34]. However, knocking down or knocking out FBL greatly reduces cell survival in most cells [33, 35, 36] (Fig. S1B–S1D), making it a challenging therapeutic target. The essential function and extensive involvement of FBL in nucleolar processes largely obscure its potential functions in pathological contexts. Surprisingly, our study revealed that FBL can be directly recruited to genomic DNA damage sites via its GAR domain under conditions

of DNA damage. This unexpected role of FBL in DNA damage repair suggests that this essential housekeeping gene fulfills an independent role under stress beyond its conventional physiological processes, acting as a pivotal driver for therapeutic resistance. Despite being known as an rRNA methyltransferase with a functional RB domain, truncation of the RB domain did not affect the DNA damage response of FBL (Fig. 2). However, depletion of the GAR domain adjacent to the RB domain completely abolished FBL's DNA damage response, leading to the loss of its regulatory function in DNA damage repair. Thus, we propose that FBL's role in DNA damage repair may represent a stress-induced novel function independent of its methyltransferase activity.

Altogether, our study uncovered the critical role of FBL in oxidative damage repair during CRC development. This elucidation of FBL's involvement in oxidative DNA damage repair highlights the necessity to further explore the uncharacterized roles of nucleolar genes under stress conditions. Furthermore, the regulation of FBL by PARP1 under DNA damage conditions offers a prospective therapeutic strategy for combining low dose radiotherapy with PARP inhibitors in CRC patients with high FBL expression.

## MATERIALS/SUBJECTS AND METHODS

### Laser micro-irradiation and analysis

A Leica DM6500 confocal microscopy 405-nm laser diode system was used for micro-irradiation. Cells were presensitized with 100 μM of 8-methoxypsoralen in medium for 2 to 5 min. DNA damage was induced by micro-irradiation with a 50 mW, 405 nm laser diode and fluorescence recovery after photobleaching model was used. At least 10-15 cells were irradiated in each experiment. Time 0 indicates frame 1 that was captured post laser immediately. The intensity of damaged points is normalized to undamaged regions that are adjacent to the damage site.

### Immunofluorescence

Cells were fixed with 4% paraformaldehyde for 15 min at room temperature, and permeabilized in 0.2% Triton X-100 for 10 min. Cells were blocked in 2% BSA for 30 min at room temperature and incubated with primary antibody at 4 °C overnight. Then washed and incubated with Alexa Fluor 488-conjugated or Alexa Fluor 594-conjugated secondary antibody (1:500) for 1 h at room temperature in the dark. Cells were stained with 1 mg/ml DAPI (1:2000) for 10 min at room temperature, washed and mounted with an anti-fade mounting medium (Vector Laboratories).

### Immunohistochemistry (IHC)

All human samples used in this study were approved by the Medical Ethics Committee of Xiangya Hospital, Central South University (ethics number: 2019030535) and informed consent was obtained from all subjects. Briefly, Paraffin-embedded specimens were cut into 4 mm sections and incubated at 60°C for at least 2 h. Sections were deparaffinized with turpentine and rehydrated. Heat-mediated antigen retrieval was performed in Sodium Citrate buffer (0.01 mol/L, pH 6.0) for 30 min. Slides were allowed to cool to room temperature and then subjected to the IHC method using a commercial kit, according to the manufacturer's instructions (Zsbio, PV-9001). Slides were incubated with primary antibody overnight at 4°C. The tissue was photographed with a multispectral microscope, and 3 fields of view were selected randomly, and the inForm 2.4.0 software (PerkinElmer) was used to automatic scoring.

### Tumor xenograft

All animal procedures were approved by the Institutional Animal Care and Use Committee (IACUC) of Central South University. Nude mice and C57BL/6 mice were purchased from Hunan SJA Laboratory Animal Co., Ltd. and mated. Mice were housed in the animal facility with a circulating air purification system in filter top, sawdust bedding cages. The cage was changed every 3 days in a laminar flow hood. Mice were feed with sterile water and nude mice specific fodder. $1 \times 10^6$ vector/ FBL overexpressed HCT8 stable cells were collected and suspended with DMEM, mixed with the same volume of matrigel and injected into the subcutaneous tissue of the flank in 6–8 weeks old, female nude mice. When tumor volumes reached 30–80 $mm^3$, mice of each cell line were randomized to 4 groups ($n = 5$) and the treatment was initiated: (1) the vehicle group (10% DMSO / 30% PEG300 / saline solution for 3 days by intraperitoneal injection); (2) the olaparib group (olaparib (50 mg/kg/day) for 3 days by intraperitoneal injection); (3) the irradiation group (10%DMSO / 30%PEG300 / saline solution for 3 days by intraperitoneal injection, tumor-localized irradiation (2 Gy) given 1 h after the dose of DMSO); (4) the combination group (olaparib (50 mg/kg/day) for 3 days by intraperitoneal injection, tumor localized irradiation (2 Gy) given 1 h after the dose of olaparib); Tumor size and body weight were measured every other day. When the tumor size got 300 $mm^3$ or the mice had severe weight loss and became moribund, mice were sacrificed and tumors were surgically dissected and tumor sizes were measured respectively. Tumor volumes were calculated by $l \times w^2/2$ (l: tumor length, w: tumor width). The investigator was fully blinded to the group allocation during the experiment and when assessing the outcome.

## DATA AVAILABILITY

The colon cancer proteomics databases used in this study are available and obtained from data portal websites (https://cptac-data-portal.georgetown.edu/cptac/s/S045; https://cptac-dataportal.georgetown.edu/cptac/s/S022). The CNA and mutation data matrices used in this study are available on the Genomic Data Commons Data Portal (GDC Data Portal) CPTAC-2 project (https://portal.gdc.cancer.gov/). Additional resources and data related to this article can be found in supplementary information or requested from the corresponding authors.

## REFERENCES

1. Gérard JP, Conroy T, Bonnetain F, Bouche O, Chapet O, Closon-Dejardin MT, et al. Preoperative radiotherapy with or without concurrent fluorouracil and leucovorin in T3-4 rectal cancers:: Results of FFCD 9203. J Clin Oncol. 2006;24:4620–5.
2. Ogura A, Konishi T, Cunningham C, Garcia-Aguilar J, Iversen H, Toda S, et al. Neoadjuvant (Chemo)radiotherapy with total mesorectal excision only is not sufficient to prevent lateral local recurrence in enlarged nodes: results of the multicenter lateral node study of patients with low cT3/4 rectal cancer. J Clin Oncol. 2019;37:33–43.
3. Forman HJ, Zhang HQ. Targeting oxidative stress in disease: promise and limitations of antioxidant therapy. Nat Rev Drug Discov. 2021;20:689–709.
4. Sharma V, Mehdi MM. Oxidative stress, inflammation and hormesis: the role of dietary and lifestyle modifications on aging. Neurochem Int. 2023;164:105490.
5. Lord CJ, Ashworth A. PARP inhibitors: Synthetic lethality in the clinic. Science. 2017;355:1152–8.
6. Jungmichel S, Rosenthal F, Altmeyer M, Lukas J, Hottiger MO, Nielsen ML. Proteome-wide identification of poly(ADP-Ribosyl)ation targets in different genotoxic stress responses. Mol Cell. 2013;52:272–85.
7. Zhang Y, Wang J, Ding M, Yu Y. Site-specific characterization of the Asp- and Glu-ADP-ribosylated proteome. Nat Methods. 2013;10:981–4.
8. Jin BL, Robertson KD. DNA methyltransferases, DNA damage repair, and cancer. Adv Exp Med Biol. 2013;754:3–29.
9. Wang XS, Huang ZY, Li L, Yang YT, Zhang JY, Wang L, et al. The role of alternative splicing factors, DDB2-related ageing and DNA damage repair in the progression and prognosis of stomach adenocarcinoma patients. Genes 2023;14:39.
10. He YJ, Meghani K, Caron MC, Yang C, Ronato DA, Bian J, et al. DYNLL1 binds to MRE11 to limit DNA end resection in BRCA1-deficient cells. Nature. 2018;563:522–6.
11. Liu H, Zhang H, Wu X, Ma D, Wu J, Wang L, et al. Nuclear cGAS suppresses DNA repair and promotes tumorigenesis. Nature. 2018;563:131–6.
12. Xie J, Wen M, Zhang J, Wang Z, Wang M, Qiu Y, et al. The roles of RNA helicases in DNA damage repair and tumorigenesis reveal precision therapeutic strategies. Cancer Res. 2022;82:872–84.

13. Shubina MY, Musinova YR, Sheval EV. Nucleolar methyltransferase fibrillarin: evolution of structure and functions. Biochem-Mosc + . 2016;81:941–50.
14. Koh CM, Gurel B, Sutcliffe S, Aryee MJ, Schultz D, Iwata T, et al. Alterations in nucleolar structure and gene expression programs in prostatic neoplasia are driven by the oncogene. Am J Pathol. 2011;178:1824–34.
15. Su H, Xu T, Ganapathy S, Shadfan M, Long M, Huang THM, et al. Elevated snoRNA biogenesis is essential in breast cancer. Oncogene. 2014;33:1348–58.
16. Vasaikar S, Huang C, Wang X, Petyuk VA, Savage SR, Wen B, et al. Proteogenomic analysis of human colon cancer reveals new therapeutic opportunities. Cell. 2019;177:1035–49 e1019.
17. Zhang B, Wang J, Wang X, Zhu J, Liu Q, Shi Z, et al. Proteogenomic characterization of human colon and rectal cancer. Nature. 2014;513:382–7.
18. Zhang L, Li Z, Skrzypczynska KM, Fang Q, Zhang W, O'Brien SA, et al. Single-cell analyses inform mechanisms of myeloid-targeted therapies in colon cancer. Cell. 2020;181:442–59 e429.
19. Nusinow DP, Szpyt J, Ghandi M, Rose CM, McDonald ER 3rd, Kalocsay M, et al. Quantitative proteomics of the cancer. Cell Line Encycl Cell. 2020;180:387–402 e316.
20. Kerppola TK. Design and implementation of bimolecular fluorescence complementation (BiFC) assays for the visualization of protein interactions in living cells. Nat Protoc. 2006;1:1278–86.
21. Dantzer F, Ame JC, Schreiber V, Nakamura J, Menissier-de Murcia J, de Murcia G. Poly(ADP-ribose) polymerase-1 activation during DNA damage and repair. Methods Enzymol. 2006;409:493–510.
22. Gibson BA, Kraus WL. New insights into the molecular and cellular functions of poly(ADP-ribose) and PARPs. Nat Rev Mol Cell Biol. 2012;13:411–24.
23. Kalisch T, Amé JC, Dantzer F, Schreiber V. New readers and interpretations of poly(ADP-ribosyl)ation. Trends Biochemical Sci. 2012;37:381–90.
24. Ahel I, Ahel D, Matsusaka T, Clark AJ, Pines J, Boulton SJ, et al. Poly(ADP-ribose)-binding zinc finger motifs in DNA repair/checkpoint proteins. Nature. 2008;451:81–U12.
25. Dani N, Stilla A, Marchegiani A, Tamburro A, Till S, Ladurner AG, et al. Combining affinity purification by ADP-ribose-binding macro domains with mass spectrometry to define the mammalian ADP-ribosyl proteome. Proc Natl Acad Sci USA. 2009;106:4243–8.
26. Karras GI, Kustatscher G, Buhecha HR, Allen MD, Pugieux C, Sait F, et al. The macro domain is an ADP-ribose binding module. EMBO J. 2005;24:1911–20.
27. Zhang H, Cai B, Geng A, Tang H, Zhang W, Li S, et al. Base excision repair but not DNA double-strand break repair is impaired in aged human adipose-derived stem cells. Aging Cell. 2019;19:e13062.
28. Olive PL, Banath JP. The comet assay: a method to measure DNA damage in individual cells. Nat Protoc. 2006;1:23–9.
29. Schreiber V, Dantzer F, Amé JC, de Murcia G. Poly(ADP-ribose):: novel functions for an old molecule. Nat Rev Mol Cell Bio. 2006;7:517–28.
30. Duan YJ, Du AY, Gu JG, Duan G, Wang C, Gui XR, et al. PARylation regulates stress granule dynamics, phase separation, and neurotoxicity of disease-related RNA-binding proteins. Cell Res. 2019;29:233–47.
31. Pandya K, Scher A, Omene C, Ganesan S, Kumar S, Ohri N, et al. Clinical efficacy of PARP inhibitors in breast cancer. Breast Cancer Res Treat. 2023;200:15–22.
32. Britton S, Dernoncourt E, Delteil C, Froment C, Schiltz O, Salles B, et al. DNA damage triggers SAF-A and RNA biogenesis factors exclusion from chromatin coupled to R-loops removal. Nucleic acids Res. 2014;42:9047–62.
33. Marcel V, Ghayad SE, Belin S, Therizols G, Morel AP, Solano-Gonzalez E, et al. p53 acts as a safeguard of translational control by regulating fibrillarin and rRNA methylation in cancer. Cancer cell. 2013;24:318–30.
34. Sun XR, Gao CW, Xu X, Li MY, Zhao XH, Wang YA, et al. FBL promotes cancer cell resistance to DNA damage and BRCA1 transcription via YBX1. EMBO reports. 2023;24:e56230.
35. Dempste JM, Rossen J, Kazachkova M, Pan J, Kugener G, Root DE, et al. Extracting biological insights from the project achilles genome-scale CRISPR screens in cancer cell lines. BioRxiv. 2017;720243.
36. Meyers RM, Bryan JG, McFarland JM, Weir BA, Sizemore AE, Xu H, et al. Computational correction of copy number effect improves specificity of CRISPR-Cas9 essentiality screens in cancer cells. Nat Genet. 2017;49:1779–84.

## ACKNOWLEDGEMENTS

This work was supported by the National Natural Science Foundation of China (81974451, 81902888, 81702956, 82030087), the Natural Science Foundation of Hunan Province for Outstanding Young Scholars (2020JJ3062), the Natural Science Foundation of Hunan Province (2023JJ40977), Innovation Foundation of Central South University for Outstanding Young Scholars (2019CX038), Award of Hunan Province for 2021 Hu Xiang Talent (2020RC3061) and Open Project Program of the State Key Laboratory of Proteomics (SKLP-O202002), the Construction of Innovative Ability of National Clinical Research Center for Geriatric Disorders (2019SK2335), the Strategy-Oriented Special Project of Central South University of China (ZLXD2017003) and Beijing Bethune Charitable Foundation (2021-YJ-088-J). National Geriatric Disease Clinical Medical Research Center clinical research Fund (2021LNJJ18). We also thank members of General Surgery Department, Xiangya Hospital for coordinating the clinical sample; members of State Key Laboratory of Proteomics, Beijing Proteome Research Center, National Center for Protein Sciences (Beijing) for assistance with the proteomic detection, Biomedical Center of Central South University Institute for Advanced Study for FACS (Flow cytometry) analysis. We thank the contribution of the specimen donors and their families.

## AUTHOR CONTRIBUTIONS

Ming Wen and YF.Q performed the major experiments and data analysis. R.T, LQ.S designed the experiments, performed the data analysis and provided the project comments. HP.P, YM.D provided the colorectal cancer patients' samples. Q.P and YQ.L collected the clinical information. A.G and ZY.M assisted the BER assay. Meng Wang, FY T, WF.H, WC.Z, ZH.C and NB.W assisted the experiments and provided technical help. R.T, Wing. Wen, YF.Q involved in manuscript preparation.

## COMPETING INTERESTS

The authors declare no competing interests.

## ETHICS STATEMENT

All methods were performed in accordance with the relevant guidelines and regulations. All human samples used in this study were approved by the Medical Ethics Committee of Xiangya Hospital, Central South University (ethics number: 2019030535) and informed consent was obtained from all subjects. All animal procedures were approved by the Institutional Animal Care and Use Committee (IACUC) of Central South University.

## ADDITIONAL INFORMATION

**Supplementary information** The online version contains supplementary material available at https://doi.org/10.1038/s41388-024-03207-w.

**Correspondence** and requests for materials should be addressed to Lunquan Sun or Rong Tan.

**Reprints and permission information** is available at http://www.nature.com/reprints

**Publisher's note** Springer Nature remains neutral with regard to jurisdictional claims in published maps and institutional affiliations.